2014-12

Morphology and Chemical Termination of HF-Etched Si_3N_4 Surfaces

UTD AUTHOR(S): Li-Hong Liu, William J. I. Debenedetti, Tatiana Peixoto, Sumeyra Gokalp Natis Shafiq, Jean-François Veyan and Yves J. Chabal

Liu, L. -H, W. J. I. Debenedetti, T. Peixoto, S. Gokalp, et al. 2014. "Morphology and chemical termination of HF-etched Si3N4 surfaces." Applied Physics Letters 105: 261603-1 to -4.

The mechanical design of a humanoid robot with flexible skin sensor for use in psychiatric therapy

Alec Burns and Yonas Tadesse
Department of Mechanical Engineering, The University of Texas at Dallas, 800 West Campbell Rd., Richardson, TX USA 75080-3021

ABSTRACT

In this paper, a humanoid robot is presented for ultimate use in the rehabilitation of children with mental disorders, such as autism. Creating affordable and efficient humanoids could assist the therapy in psychiatric disability by offering multimodal communication between the humanoid and humans. Yet, the humanoid development needs a seamless integration of artificial muscles, sensors, controllers and structures. We have designed a human-like robot that has 15 DOF, 580 mm tall and 925 mm arm span using a rapid prototyping system. The robot has a human-like appearance and movement. Flexible sensors around the arm and hands for safe human-robot interactions, and a two-wheel mobile platform for maneuverability are incorporated in the design. The robot has facial features for illustrating human-friendly behavior. The mechanical design of the robot and the characterization of the flexible sensors are presented. Comprehensive study on the upper body design, mobile base, actuators selection, electronics, and performance evaluation are included in this paper.

Keywords: characterization, humanoid, robot, assistive, rehabilitation, design, flexible sensor

1. INTRODUCTION

Psychologists or psychiatrists spend a large amount of time diagnosing an individual who has a psychological problem and then performing the necessary therapy. Humanoids, which are robots created with the human form in mind, have several applications in the areas of health care and can reduce the amount of time and effort psychiatrists need to dedicate to treating patients. Creating an affordable and efficient humanoid could assist in the therapy of psychiatric disability. In order to use humanoids in psychiatric therapy, several aspects of design, performance evaluation, cost and safety should be addressed. A fully functional humanoid needs to include the seamless integration of artificial muscles, sensors, controllers and structures which are essential to the overall performance of the robot. Artificial intelligence is the other key factor that allows the humanoid to perform a desired task in an unstructured environment. The manufacturing aspect of robots for mass production has to be considered as well. This paper seeks to look into these factors and apply them to a prototype humanoid.

The humanoid robot in this paper has 15 DOF, flexible sensors, and a mobile platform. Most parts of the robot are developed using a rapid prototyping system. The design incorporates flexible sensors, based on piezoelectric materials, embedded inside an elastomeric skin for safe human-robot interactions. The robot's face is designed to have a human-like appearance and movement. There are several humanoids capable of demonstrating emotions through facial expressions. We call them HRwFE (Humanoid Robots with Facial Expressions). These robots along with assistive robots are found to be useful in the therapy of children with autism as the robots interact with humans, demonstrating facial expressions and gestures.

The disability communication robots are useful in instantaneously teaching children with autism to correct social mistakes, by applying a real time evaluating system of a human's motion, which can help improve a child's ability to imitate human interaction [1]. It has been shown in rehabilitation robots such as KASPAR, that interacting with simple, low-cost minimally expressive robots can facilitate interactive social games that benefit children [2]. KASPAR has a static body and its design does not focus on imitating every detail of a human face[2]. This allows for the testing and development to focus on KASPAR's movements that convey communication such as eyelids, neck, and arm movements. The communication problems associated with autism vary from being unable to speak, to having a rich vocabulary but unable to pick up on social cues. Many children with autism have problems with word and sentence meaning, intonation, and rhythm; and require nonverbal communication to help them interact with others[3]. Nonverbal communication

Electroactive Polymer Actuators and Devices (EAPAD) 2014, edited by Yoseph Bar-Cohen, Proc. of SPIE
Vol. 9056, 90562H · © 2014 SPIE · CCC code: 0277-786X/14/$18 · doi: 10.1117/12.2046470

involves a combination of gestures, body language, facial expressions, and emotions. Children with autism disability lack social interactions and exhibit various symptoms.

The assistive robot communicates with children in a social manner; therefore, it is important for the robot to have a perception of humanness. The top three vital features in the design of a humanoid head are the eyes, mouth, and heads. But the features that have a statistically significant effect on the perception of humanness are the mouth, nose, and eyelids [4]. These features do not always have to be incorporated into the design of a humanoid to convey emotion, but it makes it easier for a child to associate with the robot if it does. Assistive robots have laser range finders, sonar sensors, microphones for speech recognition, speakers for speech synthesis, and touch-sensitive graphical displays that allow input from nurses and medical experts.

Combining the two abilities of both robots allowed us to design a robot with both rehabilitation and assisting qualities in mind. As medical science advances and a rising population ages, there will become a need for assistive robots. Some countries invest a huge amount of scientific research in the area of humanoids. This can be seen in Japan's large investment in personal robotics in relation to their significant proportion of elderly Japanese [5]. These assistive robots are usually meant to provide a fetch-and-carry service rather than serve a cognitive function. A robot in home care for the elderly, called Pert was able to help individuals remember appointments, television schedules, and weather reports [6]. To accomplish this goal, while maintaining the appropriate strength, the design was loosely based off of human anatomy.

2. MECHANICAL DESIGN

The rehabilitation robot for use in psychiatric therapy is shown in figure 1. The robot consists of a two wheeled mobile base, a cloud camera, ultrasonic position sensor, battery, wireless communication module, flexible touch sensor skin, two 4 DOF arms, a 5 DOF head and a 2 DOF neck. The overall dimensions of the robot are a height of 580 mm, an arm space of 925 mm, shoulder width of 230 mm, and a chest thickness of 172.5 mm. The mechanical design considered a few key concepts such as: symmetry of parts, axial alignment of different joints, and easily accessible actuators that can be removed or replaced for maintenance. The overarching theme involved in these concepts was based on maximizing the number of parts to be 3D printed, so that the design would not have to rely on other venders or machine shops. These 3D printed parts can be put together in such a way that users can easily replace parts that are either broken, or require a change in geometry. Most of the robot's parts are fabricated using ABS (Acrylonitrile Butadiene Styrene) plastic material using 3D printer. The strength of ABS plastic is 32 to 45 MPa [7]. Therefore the maximum load that can be carried should account the geometrical as well as strength of the 3D printed ABS material properties. To accomplish this goal, while maintaining the appropriate strength, we used bolts and nuts to assemble the 3D printed parts.

2.1 Upper Body Design

The torso of the robot was designed to mimic the rib cage and spine of a human. Three rectangular prims that serve as a protection for the center column of the torso were made in a similar manner that the ribs do for humans. Also, like a human spine, the center column of the torso was designed not only to ensure that the robot is stable and rigidly connected to the mobile base, but was also designed so that wires and any other electronic equipment can be routed through it. This allows easy access between the power supply and on board computational equipment in the base to safely be connected to all actuators located at the top of the torso with minimal wire. The torso was also covered in wide array of 2.5 mm

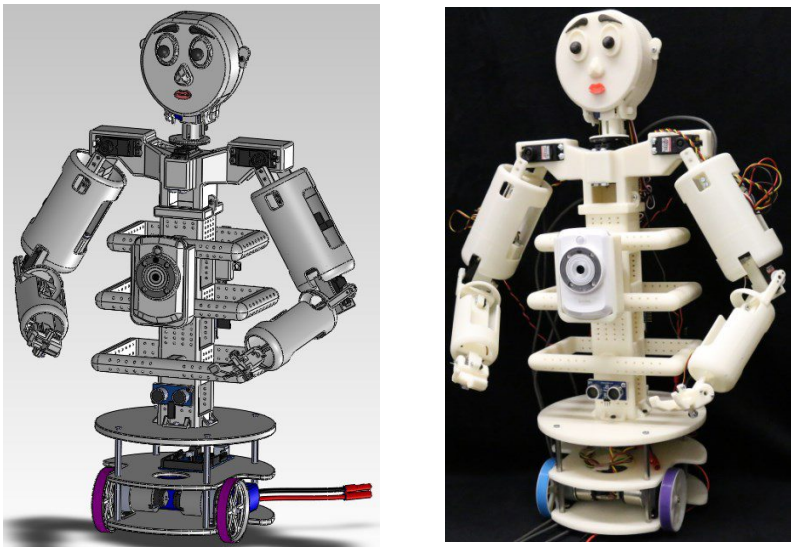

Figure 1. Robot with bent arms; SolidWorks model, assembled prototype.

diameter holes, which serves for multiple purposes, one of which is to reduce the weight while maintaining structural integrity similar to the lattice structure in human bones. The other purpose of these holes is to serve as an easy way to mount different sensors, and electronics. The shoulders were designed as a single 3D printed piece that would slide on the top of the torso and attached with two bolts. The purpose of the shoulders was to house the actuators for the arms and a mount for the flexible skin cover. Servo motors were chosen as the main actuators, and as such the design had to fit the servos almost perfectly to allow them to slide in and out for maintenance.

The face was designed to show five basic emotions, happiness, sadness, anger, fear, and disgust. The most mechanically complex part of the robot was the head and features on the face. As stated earlier, the intended use of the robot was to express emotions when interacting with children. To facilitate this, we designed the head of the robot with moveable eyes, eyebrows, and mouth. The eyes give the robot a more life-like feel and the eyebrows help convey emotion to others. These portions of the design were complex because they required the creation of 3D printed spur gears, as well as 3D printed rack and pinion gears. This was done so that the head could be operated with a minimum number of servos.

The hand was also designed to grasp a variety of objects and can be easily redesigned and replaced. The method that was used to allow the easy replacement of servos was to incorporate a peg-in-hole structure. The structures were created in the arms using SolidWorks CAD software. Each part of the arm was then printed in two parts: one part to slide onto the peg and the other part to be bolted to the servo's rotor. These two parts were then bolted together to create one stable arm. Once the arm was designed, an aesthetic portion was added to the outside of it. As observed in Figure 1 the aesthetic used was a simple cylinder. The aesthetic can be redesigned to appeal to the subject that it works with. In addition, flexible sensors that cover the arm can be mounted at this portion. The hands have one thumb, and instead of four fingers, it has one wide finger. Several bolts were used in the arms and hands for mounting servo motors.

2.2 Mobile Base

In contrast to the design of the upper body, the mobile base abandoned the idea of mimicking the human anatomy. The mobile base was designed so that the robot could quickly move around a hospital or therapy room without the required complexity of a human leg. A three tier design was chosen for the mobile bases which included sensors for navigation. This enabled the main body to be taken off and worked on separately, and provided enough space on its mid and bottom tiers to hold all necessary electronics for the robot. The base design as shown in Figure 2(a) included: two 3D printed front wheels, stainless steel standoffs, a 3D printed rear skid, and rubber wrist bands for wheel traction. After the base was designed in SolidWorks, simulations were performed to analyze the stress and displacement of the base to check the load carrying capacity. The simulations were done assuming that the upper body of the robot does not exceed 10 kg. The skid touches and wheel mounts were assumed to be fixed with the ground for this simulation. Then, the stress simulations were carried out. As depicted in Figure 2(b) the maximum stress were found to be at the stainless steel standoffs with a magnitude of 262 MPa. The maximum displacement was found to be in the center of the top tier with a magnitude of 2.19 mm. The other crucial 3D printed part that required simulation for the base was the 3D printed wheels. It was assumed that each wheel could support a one third of the total 10 kg of weight on it, since there were three points of contact between the mobile base and the ground. After the simulation, it was found out that the maximum stress was 1.50 MPa, and the maximum displacement was 0.013 mm. Both of these simulations showed that the 3D printed parts were safe enough to carry the load under normal operating conditions. It is to be noted that the tensile strengths of typical ABS plastic used in 3D printing range from 32 to 45 MPa[7] .

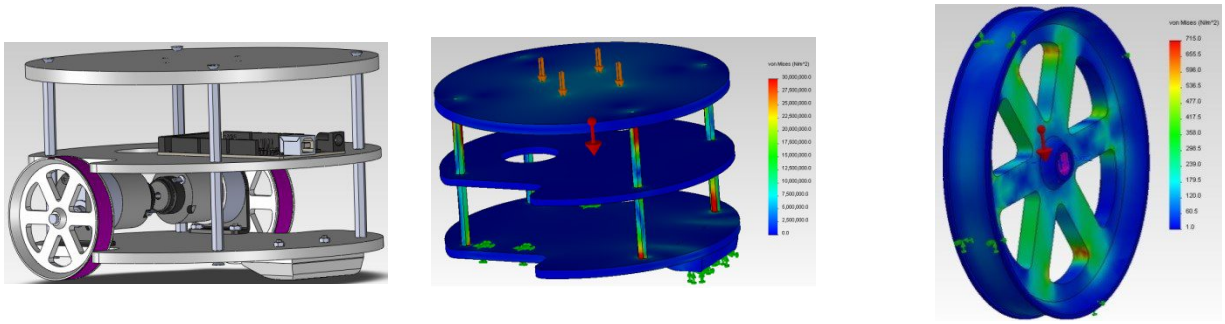

Figure 2. Mobile base of the robot: (a) SolidWorks assembly, (b) Stress simulation of the mobile base and (c) stress on the wheel.

2.3 Joint Actuator Selection

To actuate such 3D printed materials, we considered various actuators including servo motors, DC motors with cables, and shape memory alloy (SMA). SMAs are the most commonly used for confined space applications in biomimetic systems and humanoids, but they require pulley systems that must be housed and anchored inside the each part [8,9]. While SMAs are excellent compared to other actuators, they lack a built in measurement system, which adds to the complexity of their implementation. RC servos are usually used for low torque applications that require a high degree of precision and easy control. This high degree of precision is accomplished because servo motors have built in encoders or position sensors that allow the user to measure their rotation in real time. Since the robot will be dealing with children in therapy the actuators should generate minimized noise, and no sudden or dramatic movements. The noise can be avoided using lubricants [10] or noise suppression box [11]. These factors led to the decision of using servos as our robotic actuators, and DC motors for the mobile base actuators mainly due to controlling issues. The shoulder and elbow actuators required high torque depending on what object is being manipulated by the robots arms. The first thing for the design of the 3D printed parts was to ensure perfect fitting inside designed slot. The torque and speed of servo motors were calculated and selected from the commercially available venders and then each servo was meticulously recreated into a SolidWorks model keeping exact dimension. In similar fashion, a wireless camera, an ultrasonic sensor, and many bolts and nuts were designed and manufactured using rapid prototyping as shown in in Figure 1.

2.4 Mechatronics components

The mechatronics components of the robot were actuators (DC motors, RC servo motors), encoders, controllers (Arduino Mega, Maestro controllers), step-down voltage regulators, Xbee wireless communication module, wireless cloud camera, and lithium polymer battery. These components took 56% of the total material cost of the robot. As seen in Figure 3, the mechatronic components costs were approximately $2,000, higher than all other portions of the robot combined together. These parts of a robot truly define how capable a robot is in performing desired tasks, especially, for our robot designed to interact with children. Therefore, having servos motor at each joint is not sufficient enough to allow for human interaction. There are 13 different servo motors, and they all need to communicate together to create smooth motion, and ensure that no one is harmed as well.

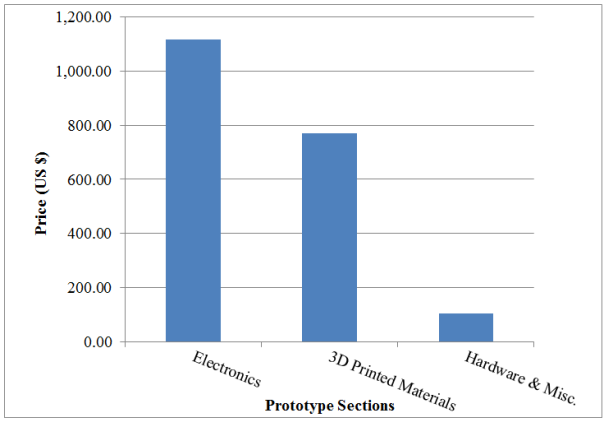

Fig. 3 Cost of each section of the prototype robot

Three Micro Maestro 6-Channel USB servo controllers were used to measure and regulate the speed, acceleration, and position of servos in three sections of the robot; the head and neck, the left arm and hand, and the right arm and hand. These servo controllers were found to be useful due to the three types of control methods; USB connection, TTL serial, and internal scripting for self-contained applications [10]. In order to control the servos separately, the servo controllers were connected to a single-board microcontroller, Arduino Mega 2560 REV3. The Arduino Mega was enough to support communication with three servo controllers since it has 4 hardware serial ports. The Arduino hardware was programmed using a wiring-based language (syntax and libraries), similar to C++ with some slight simplifications and modifications, and a processing-based integrated development environment [12]. The Arduino was programmed using Arduino IDE that has been developed using Java, and other open source software [12]. The DC motors that actuate the mobile base of the robot were gear head motors with gear reduction ratio of 30:1, a maximum speed of 291 rpm, and a stall torque of 3.9 kg-cm. The torque was sufficient to be able to move the robot, and any object that it might be carrying. The DC motors were controlled through a L293D Motor Driver chip which was in turn controlled by the Arduino Mega.

The voltage consumption of the DC motors, the servo controller and the Arduino Mega were 7.2, 6, and 5 volts respectively, which can be powered through an external power supply. This was beneficial to the robot since it is a mobile robot, and cannot be reliant on a wired power source. The most often used energy sources are rechargeable batteries, but they need to be recharged after exhaustion [13]. A battery pack was used for the mobile base that has a capacity to store a 4400 mAh (SKY LIPO 4400mAh 40C 11.1V Hardcase Lipo Battery Pack) to provide power to all the electronics as laid out by Figure 4. This rechargeable battery was perfect for the mobile robot since it can be replaced and

recharged in a short period of time, and it has enough power to operate all necessary electronics. Pololu Step-Down voltage regulators (D15V70F5S3) were used to reduce the voltage required to the servo controllers.

Sensors do not require a large amount of power and it is necessary to include them in any capable robot. For dealing with children the robot needs to always be aware of its surroundings, and react appropriately. For this reason we incorporated a Parallax PING ultrasonic sensor, a D-Link DCS-942L enhanced wireless day/night home network camera, and a flexible piezoelectric sensing array. This camera is mounted onto the front of the robot's torso and allows the robot to use visual sensing to decide the next correct motion. This could involve observing visual cues from the child to decide the robot's emotional expression, or could help with facial tracking which would allow the robot to follow a child around or just have its eyes looking in the correct direction. The ultrasonic sensor is a more static sensing, it sends out a ping and then measures the time for it to return, this can be used to measure the distance from the sensor to what it is sensing. The ultrasonic sensor is mounted on the bottom on the torso and would be used to constantly ensure that the robot is running into obstacles which could include: walls, chairs, or other children.

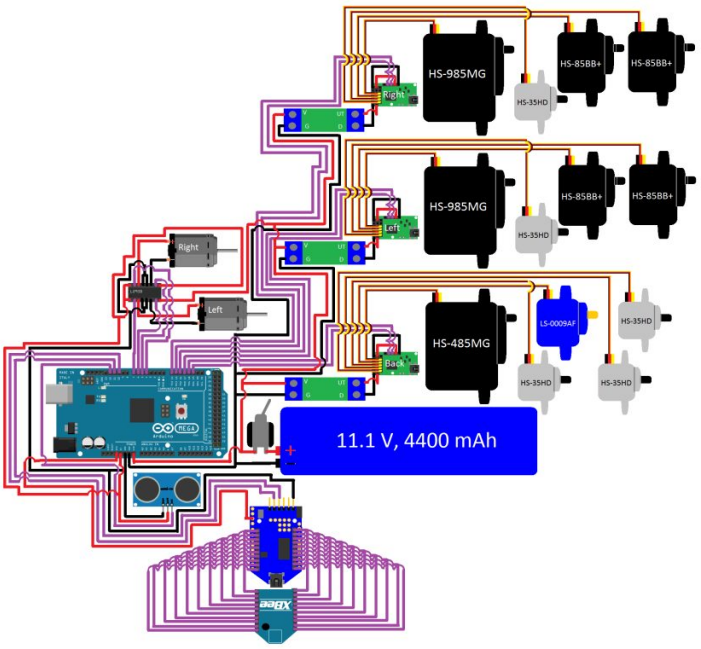

Figure 4. Wiring Diagram for the robotic prototype

2.5 Manufacturing

Most sensors required the manufacturing of a unique mount to attach to the robot; fused deposition (FDM) rapid prototyping was used. The total time and the volume of materials used in making the parts are shown in Figure 5. The rapid prototyping has several advantages to create complex geometries and in relatively short period of time. The main issue for designing a 3D printed part to perfect fit around equipment is that each 3D printer has a certain tolerance associated with it. Other problems with 3D printing as seen from Figure 5 are that the manufacturing time is fairly large for a small volume of material, but this large manufacturing allows for the development of complex shapes and designs to be utilized. The robot was 3D printed using the Stratasys Dimension Elite 3D printer which has a minimum printable feature size of around 0.178 mm; which is the size of one layer of ABS Plastic also called the bead width. The surface roughness of 3D printed parts also plays a significant role in moving parts causing friction and restricting motion. To minimize this result, many versions of a rectangular prism were printed with various size gaps between the servo and the 3D printed part as seen in Figure 6. After testing the friction between the parts, it was found that leaving a distance of 0.2 mm between parts that are meant to move would minimize the friction and allow the parts to move.

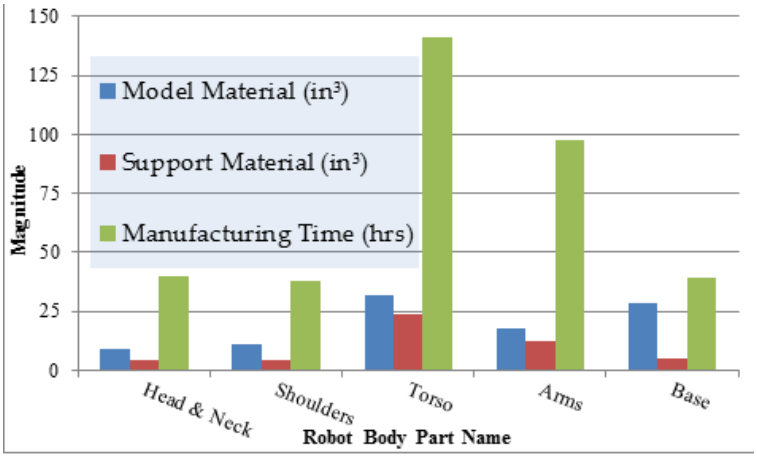

Figure 5. Manufacturing time, model material, and support material for each part of the robot.

When testing parts that are designed to rotate, it was noticed that 3D printed parts tend to be weaker than fully casted parts for a variety of reasons. To minimize the chances of our parts being 3D printed with less than desirable strength, we followed the following rules when printing our parts for the robot: (1) build parts such that tensile loads are carried axially along the fibers, (2) the wall thickness of a part should be an integer multiple of the bead width to avoid gaps, (3) avoid sharp corners and small fillet radius – be aware that stress concentrations occur at corners because the Fused Deposition Method of 3D printing exhibits discontinuities at such transitions and (4) build orientation for strength and part accuracy[7].

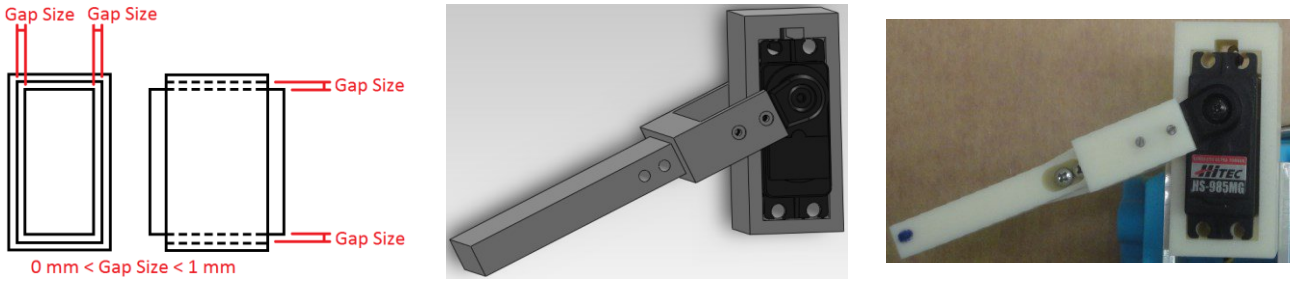

Figure 6. Gap testing for 3D printed fittings (a) gap size in two views, (b) CAD model of servo and (c) prototype

2.6 Skin Sensor

Another way to ensure that the robot is not put in a situation where strength of the design is an issue is to have skin sensors developed for the robot. These sensors are based on piezoelectric materials embedded within elastomeric substrate. Piezoelectricity is a phenomenon exhibited by non-centrosymmetric crystals whereby an electric polarization (i.e. charge) is induced in the material upon the application of a stress. This is called the direct effect and is used in sensing dynamic pressure changes, changes in acceleration (from shock or vibration), and changes in force[14]. The bulk of the piezoelectric materials used for commercial sensing applications come from synthetic polycrystalline ferroelectric ceramics, such as Lead Zirconate Titanate (PZT) ceramics [14].

The artificial skin sensor was fabricated by placing PZT discs in a rectangular array and then casting Ecoflex rubber by mixing part A and B. The Ecoflex Rubber used was Ecoflex 00-10, and is a platinum-catalyzed silicone that is mixed by weight or volume and cured at room temperature with negligible shrinkage. The resultant cured rubber is naturally translucent, soft, strong and has the ability to stretch up to 900% of its length without tearing [15]. This creates a soft, but flexible, and moldable skin-like sensor. The PZTs(diameter 10mm and 0.2 mm thick) embedded in this sensor creates a voltage when a pressure is applied on them, similar to the way nerve cells in humans create a charge to sense pain on their skin. As seen in Figure 7(a), the skin sensor was applied to the robot's arm to provide a soft contact between the user and the robot. This sensing array can then be applied to all portions of the robot. Not only will this create a soft surface to protect children from the rough surface of the 3D printed ABS plastic, but it also allows the robot to further expand its obstacle avoid capabilities. When a child touches this artificial skin, the robot will immediately know the location of the touching, and its magnitude. The robot can then pull away or prevent other movements from intersecting that location and hitting the child. Figure 7(b) and (c) show the array of PZT sensors with the connection wires before the elastomer is cast and after. While flexible sensors allow the robot to avoid undesirable events, it is not the deciding factor that allows the robot to accomplish its intended actions.

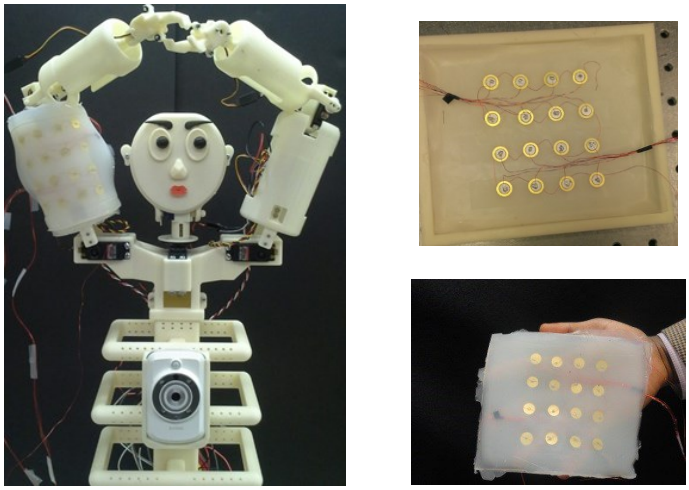

Figure 7. (a) Flexible sensor applied to the arm of the robot, (b) PZT array (c) PZT embedded inside elastomer.

3. MODELING

3.1 Pose

Gestures for a robot can be based on task oriented goals, such as getting the child an object. Since the robot will be dealing with children it should capable of gestures that could convey some type of emotion to a child. Such gestures would include waving hello or goodbye. Before designing a humanoid robot, it must be decided what kind of poses would be useful for its intended purposes.

3.2 Applying the DH Convention

After deciding the required poses the robot's links and actuators should be decided. This will help ensure that all possible positions of the robots hand can reach the intended poses; this is called the workspace of the robot. The Denavit-Hartenberg (DH) Convention is widely used in the robotic industry, and allows the position and orientation of an end effector to be represented in terms of rotations and translations related to a base coordinate system[16]. This is done using homogeneous transformation matrices to transform a coordinate system from one joint of a robot's arm to another. Each homogeneous joint transformation is represented as a product of four basic transformations: a rotation of angle θ around the current z-axis which is given as:

$$T_{\theta_{z_i}} = \begin{bmatrix} \cos(\theta_i) & -\sin(\theta_i) & 0 & 0 \\ \sin(\theta_i) & \cos(\theta_i) & 0 & 0 \\ 0 & 0 & 1 & 0 \\ 0 & 0 & 0 & 1 \end{bmatrix} \quad (1)$$

A translation of distance "d" along the current z-axis described in matrix form as:

$$T_{d_{z_i}} = \begin{bmatrix} 1 & 0 & 0 & 0 \\ 0 & 1 & 0 & 0 \\ 0 & 0 & 1 & d_i \\ 0 & 0 & 0 & 1 \end{bmatrix} \quad (2)$$

A translation of distance "a" along the new x-axis written as:

$$T_{a_{x_i}} = \begin{bmatrix} 1 & 0 & 0 & a_i \\ 0 & 1 & 0 & 0 \\ 0 & 0 & 1 & 0 \\ 0 & 0 & 0 & 1 \end{bmatrix} \quad (3)$$

A rotation of angle α around the new x-axis described as:

$$T_{\alpha_{x_i}} = \begin{bmatrix} 1 & 0 & 0 & 0 \\ 0 & \cos(\alpha_i) & \cos(\alpha_i) & 0 \\ 0 & \cos(\alpha_i) & \cos(\alpha_i) & 0 \\ 0 & 0 & 0 & 1 \end{bmatrix} \quad (4)$$

The product of the matrix from Eq. (1)-(4) then becomes the transformation matrix for each joint in the robots arm which is obtained as:

$$T_i = \begin{bmatrix} \cos(\theta_i) & -\cos(\alpha_i)\sin(\theta_i) & \sin(\alpha_i)\sin(\theta_i) & a_i\cos(\theta_i) \\ \sin(\theta_i) & \cos(\alpha_i)\cos(\theta_i) & -\sin(\alpha_i)\cos(\theta_i) & a_i\sin(\theta_i) \\ 0 & \sin(\alpha_i) & \cos(\alpha_i) & d_i \\ 0 & 0 & 0 & 1 \end{bmatrix} \quad (5)$$

Each joint transformation is then multiplied together, in order from first joint to the end effector, resulting in a matrix that is unique to the designed robot, and can describe the end effector in terms of the base coordinate system. This matrix description includes both location and orientation for which we can use to evaluate the design of a humanoid robot. Before determining the homogeneous transformation matrices, the origin and axes for each joint needs to be selected. Since the robot is mounted on top of a mobile base, it was decided that the top of the mobile base would serve as the base coordinate system for the robotic arms modeling. The robot is human-like; therefore, the general placement of the joints can be easily done by mimicking a human arm. The human arm has 6 DOF, but to reduce the complexity of the robot hand, we did not include the roll movement of a human shoulder and the twisting movement of the human forearm.

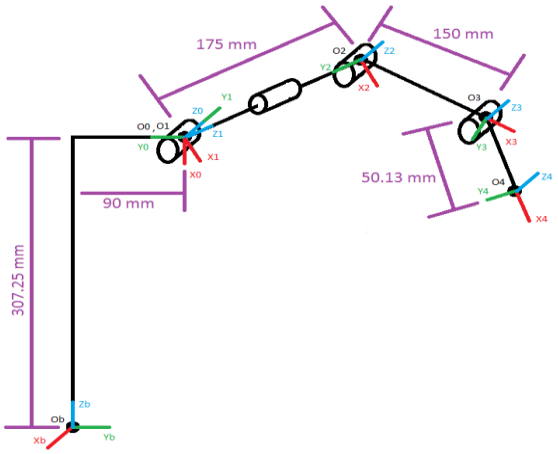

Figure 8. The robots arm with the applied DH Convention for coordinate axes.

Table 1. DH Parameters that related to each joint axes

Link	α_x(deg)	a_x	d_z	θ_z
1	90	0	0	θ_1
2	-90	0	d_2	θ_2
3	0	a_3	0	θ_3
4	0	a_4	0	θ_4

As seen in Figure 8, lengths were estimated between the joints that satisfy the size of the robots. By following the DH convention, the axes for each joint were placed in their appropriate places and are shown in Figure 8. Using the known joint axes, and estimated lengths a set of DH Parameters can be created to calculate the homogeneous transformation matrix of each joint. These parameters can be seen in Table 1. To make sure that the robot was modeled correctly, Matlab was used to compute and plot each joint and corresponding joint axes. This was done to confirm that the individual joint transformations were determined correctly, the Matlab generated graph can be seen in Figure 9. Since the Matlab graph of the robot's arm and coordinate systems match the earlier defined axes from the DH Convention, it is confirmed that the DH Convention was applied properly.

3.3 Workspace Analysis

From the Matlab model and the final joint transformation, the location of the end effector with respect to the base frame was used to create the workspace of the robot. This resulted in an equation for the x, y, and z locations of the end effector in terms of the rotation of each actuator. If the joint actuator limitations are known (as is the case with the robot we are designing); then the use of these rotation limits, and the equations of the end effector can be used to model all possible locations of the end effector. This calculation was done using Matlab. The visualization of this workspace volume can be seen in Figure 10 which includes the movement of both arms of the robot. Inspection of Figure 10 shows that the arms are able to touch each other when the end effector is located above the shoulders of the robot. After a manipulator has been normalized, for example with respect to its maximum reach, it can be evaluated or optimized in terms of workspace volume [16]. This optimization is left out for future work.

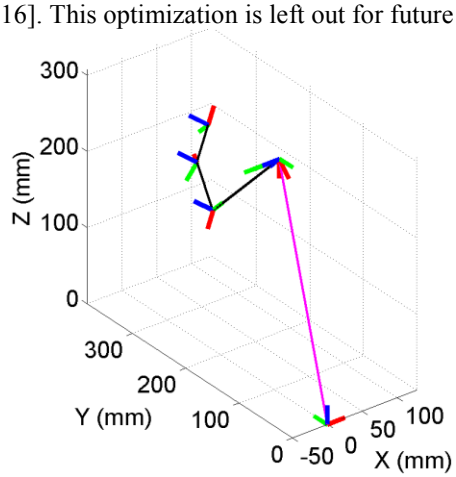

Figure 9. Matlab generated model of the DH Convention for our robots arm

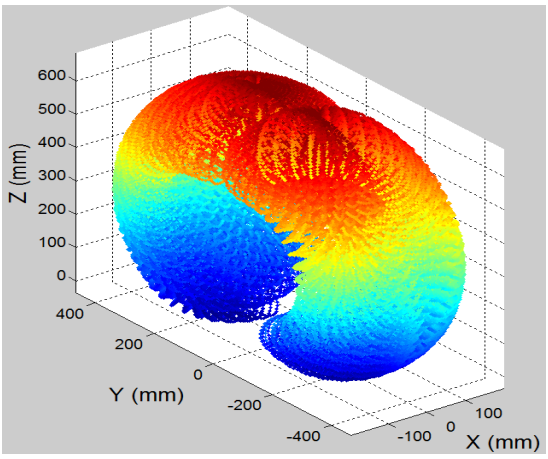

Figure 10. Workspace for both arms of our robot.

4. EVALUATION

To evaluate the robot's ability to interact with others, we tested its movement and ability to convey emotion to others. The joints were actuated by the corresponding servo motors using Maestro programming interface. As seen in Figure 11, the full range of motion for the robot's arms and hands allows it to hold objects in two hands, point, and even play certain games involving gestures. Figure 11(a) is the normal appearance; 11(b) is when the arms are stretched forward; 11(c) is both arms raised up; 11(d) both arms stretched wide (getting ready to hug); and 11(e) the arms are folded.

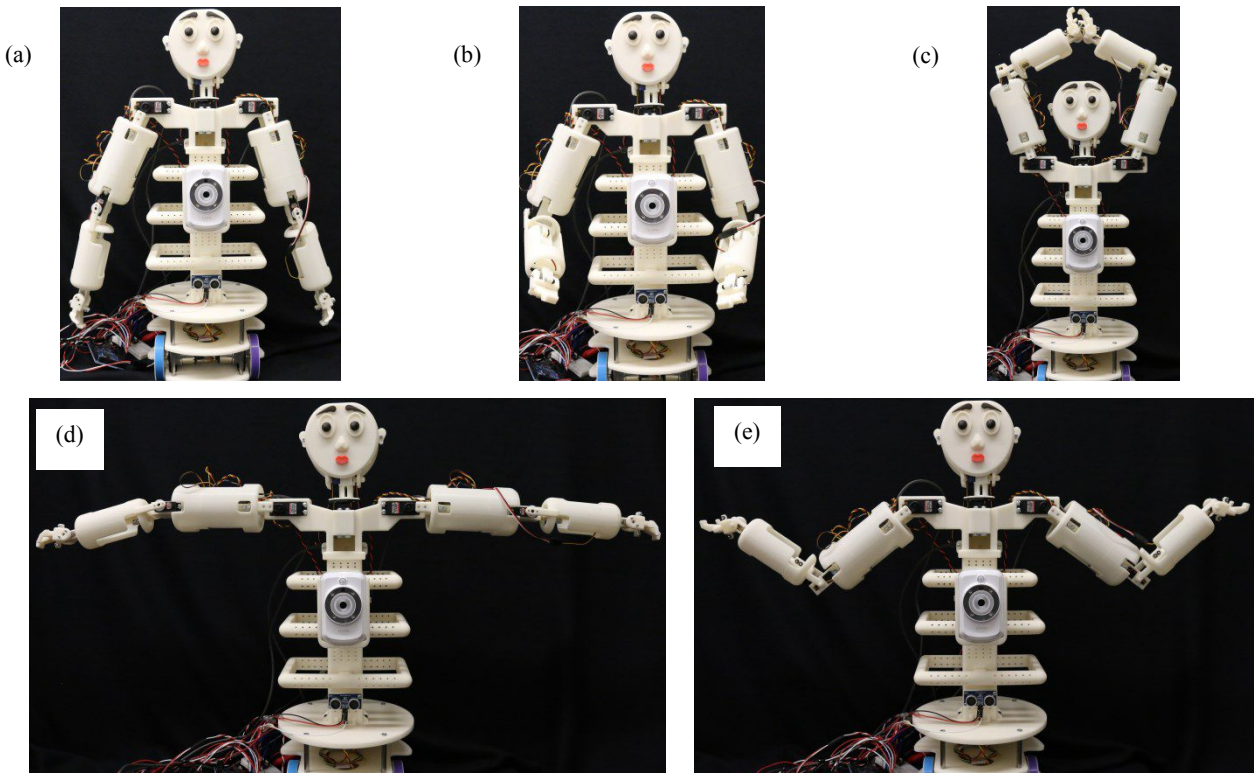

Figure 11. The robots range of arm motion.

To test the robot's ability to show emotion, we tested all movements that involved the head and facial features such as: the eyebrows, eyes, mouth, and neck movements. The pictures in Figure 12 are some of the possible facial expressions shown by the robot. When the eyebrows are pointed up, the robot shows a look of concern or sadness, while when the eyebrows are pointed down the robot's face shows a look of anger or frustration. These simple expressions of emotion from the facial features can be amplified when paired with the robot's neck movements. Having the eyebrows pointed up while also having the head tilted down can show an expression of grief while having the head tiled upwards can convey hopefulness. The face shows comparable emotions similar to those robot heads made of elastomeric skin [18]. The face shows comparable emotions similar to those robot heads made of elastomeric skin [9]. An added capability of showing emotion is to tie the emotion to when an unwanted event has occurred, such as touching the robot too hard.

Figure 12. The robots range of racial expressions (a) normal, (b) scared, (c) concern or sad, (d) grief and (e) hopefulness

A single PZT that was embedded in the silicone flexible skin was tested to evaluate the skin's sensitivity at various distances away from its center. The test was conducted by placing a constant mass of 400 grams in four locations relative to the center of the PZT at increments of 5 mm. The dimension of the skin was 167.64 mm long, 142.24 mm wide and 5.21 mm thick. The PZT was 2.54 mm below the top skin surface. As seen in the inset of Figure 13, the skin was subdivided into 8 areas and the load was applied at each areas. The magnitude of the maximum voltage output of the sensor at a distance of 5mm, 10 mm, 15mm and 20 mm were 0.3, 0.2, 0.6, and 0.2 V respectively. The variation of the voltage was attributed to the magnitude of stress applied on the PZT, inconsistency in applying the load and the non-uniformity of the elastomer. It was found that if the force is applied 15 mm away from the center of the PZT, then it will result in the largest voltage response from the PZT. Also seen in Fig. 13, the maximum voltage produced was approximately 0.6 volts, which is sufficient enough for a simple microcontroller such as an Arduino Mega to sense. In the future with enough silicon elastomer, it would even be possible to cover the entire humanoid robot with this flexible skin sensor.

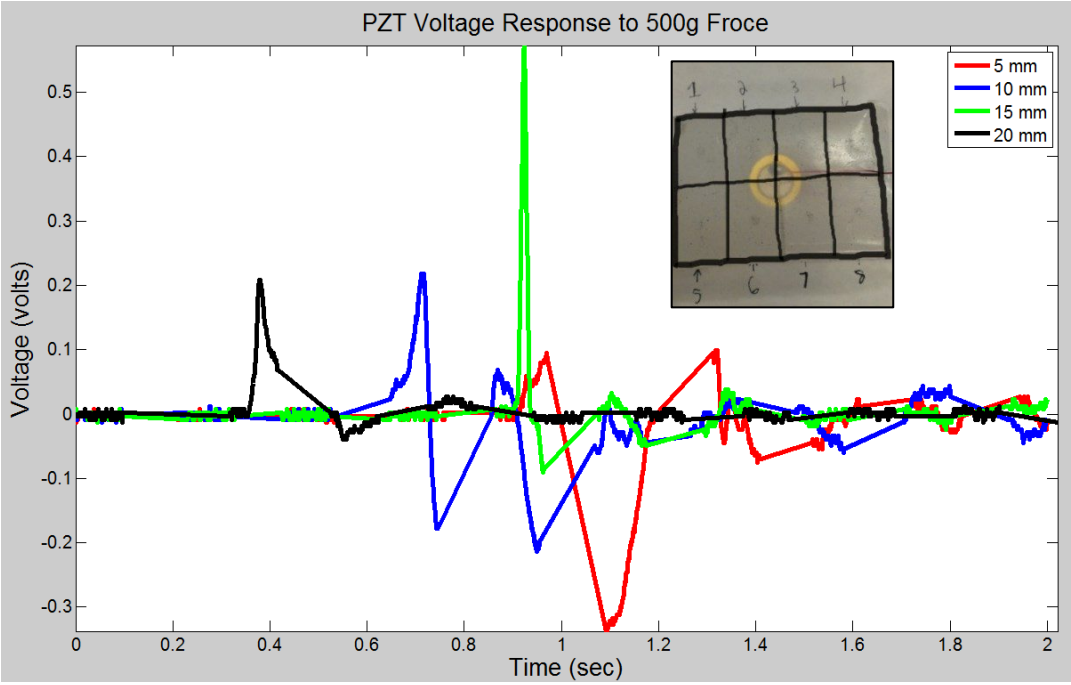

Figure 13. Force testing the flexible sensor in different locations

5. CONCLUSION

In this study the design of a human-like, full humanoid robot with 15 DOF, and a mobile platform was presented. The design elements of the upper body, mobile base, mechatronic components, were discussed in detail. Almost all parts of the robots are 3D printed and the accurate placements of components provided successful articulation of the robot's joints as desired. The evaluation of the robot was found to demonstrate the capabilities required for assistive and rehabilitation therapy. The robot was able to show facial expressions and emotions illustrating human-friendly behavior, as well as track and follow an object around. The modeling of the robot and the application of flexible sensors were also presented. The DH Convention was utilized to determine the reachable position (workspace). For the robot designed, the workspace was found for each arm, and it was seen that the arms are able to touch each other when above the head of the robot. The robot's arm was equipped with flexible PZT sensors embedded in silicone elastomer. The sensors' responses were sufficient to be captured by microcontroller. This allowed the robot to be sensitive to its environment and react accordingly to the touching of its arm.

REFERENCES

[1] Fujimoto, I., Matsumoto, T., De Silva, P Ravindra S, Kobayashi, M. and Higashi, M. , "Mimicking and evaluating human motion to improve the imitation skill of children with autism through a robot," International Journal of Social Robotics 3(4), 349-357 (2011).

[2] Robins, B., Dautenhahn, K. and Dickerson, P., "From isolation to communication: a case study evaluation of robot assisted play for children with autism with a minimally expressive humanoid robot," Advances in Computer-Human Interactions, 2009. ACHI'09. Second International Conferences on, 205-211 (2009).

[3] Pioggia, G., Sica, M. L., Ferro, M., Casalini, S., Igliozzi, R., Muratori, F., Ahluwalia, A. and De Rossi, D. , "Facial Automaton for Conveying Emotions as a Social Rehabilitation Tool for People with Autism," Itech Education and Publishing, Vienna (2007).

[4] DiSalvo, C. F., Gemperle, F., Forlizzi, J. and Kiesler, S., "All robots are not created equal: the design and perception of humanoid robot heads," Proceedings of the 4th conference on Designing interactive systems: processes, practices, methods, and techniques, 321-326 (2002).

[5] Fong, T., Nourbakhsh, I. and Dautenhahn, K. , "A survey of socially interactive robots," Robotics and autonomous systems 42(3), 143-166 (2003).

[6] Pineau, J., Montemerlo, M., Pollack, M., Roy, N. and Thrun, S. , "Towards robotic assistants in nursing homes: Challenges and results," Robotics and Autonomous Systems 42(3), 271-281 (2003).

[7] Ahn, S., Montero, M., Odell, D., Roundy, S. and Wright, P. K. , "Anisotropic material properties of fused deposition modeling ABS," Rapid Prototyping Journal 8(4), 248-257 (2002).

[8] Tadesse, Y., "Electroactive polymer and shape memory alloy actuators in biomimetics and humanoids," SPIE Smart Structures and Materials Nondestructive Evaluation and Health Monitoring, 868709-868709-12 (2013).

[9] Tadesse, Y. and Priya, S. , "Graphical Facial Expression Analysis and Design Method: An Approach to Determine Humanoid Skin Deformation," Journal of Mechanisms and Robotics 4(2), 021010 (2012).

[10] Potnuru, A. Low noise, interactive robotic system for psychiatric rehabilitation of children (2013).

[11] Gao, B., Xu, J., Zhao, J., Xi, N., Shen, Y. and Yang, R. , "A Humanoid Neck System Featuring Low Motion-Noise," Journal of Intelligent & Robotic Systems 67(2), 101-116 (2012).

[12] Yusoff, M. A. K., Samin, R. E. and Ibrahim, B. S. K. , "Wireless Mobile Robotic Arm," Procedia Engineering 41, 1072-1078 (2012).

[13] Mei, Y., Lu, Y., Hu, Y. C. and Lee, C. G., "A case study of mobile robot's energy consumption and conservation techniques," Advanced Robotics, 2005. ICAR'05. Proceedings., 12th International Conference on, 492-497 (2005).

[14] Tressler, J. F., Alkoy, S. and Newnham, R. E. , "Piezoelectric sensors and sensor materials," Journal of Electroceramics 2(4), 257-272 (1998).

[15] Aldalali, B., Fernandes, J., Almoallem, Y. and Jiang, H. , "Flexible Miniaturized Camera Array Inspired by Natural Visual Systems," (2013).

[16] Spong, M. W., Hutchinson, S. and Vidyasagar, M., [Robot Modeling and Control], John Wiley & Sons New York (2006).

[17] Gupta, K. , "On the nature of robot workspace," The International journal of robotics research 5(2), 112-121 (1986).

[18] Hanson, D., Bergs, R., Tadesse, Y., White, V. and Priya, S., "Enhancement of EAP actuated facial expressions by designed chamber geometry in elastomers," Smart Structures and Materials, 616806-616806-9 (2006).